

The synthesis, characterization and properties of alkyl complexes of the type $[\text{Cp}^*\text{Fe}(\text{CO})_2\text{R}]$ ($\text{Cp}^* = \eta^5\text{-C}_5(\text{CH}_3)_5$; $\text{R} = n\text{-C}_3\text{H}_7$ to $n\text{-C}_{12}\text{H}_{25}$); the X-ray crystal and molecular structure of $[\text{Cp}^*\text{Fe}(\text{CO})_2(n\text{-C}_5\text{H}_{11})]$ and molecular orbital and density functional calculations on the β -hydride elimination of $[\text{CpFe}(\text{CO})_2(\text{CH}_2\text{CH}_3)]$

R. Oliver Hill, Charles F. Marais, John R. Moss*, Kevin J. Naidoo¹

Department of Chemistry, University of Cape Town, Rondebosch 7701, Capetown, South Africa

Received 5 May 1999; received in revised form 5 May 1999

Abstract

The alkyl compounds $[\text{Cp}^*\text{Fe}(\text{CO})_2\text{R}]$ have been synthesized by the reaction of $\text{Na}[\text{Cp}^*\text{Fe}(\text{CO})_2]$ with the appropriate n -alkyl chloride or bromide ($\text{Cp}^* = \eta^5\text{-C}_5(\text{CH}_3)_5$; $\text{R} = n\text{-C}_3\text{H}_7$ to $n\text{-C}_{12}\text{H}_{25}$). The majority of the compounds are new and have been fully characterized by microanalysis, IR, ^1H -, and ^{13}C -NMR and mass spectrometry. The data are discussed and some properties of the compounds are described. The X-ray crystal and molecular structure of $[\text{Cp}^*\text{Fe}(\text{CO})_2(n\text{-C}_5\text{H}_{11})]$ has been determined. The compound forms monoclinic crystals in the space group $P2_1/c$ and has a Fe–C(alkyl) bond length of 2.07 Å. The structure and β -hydride elimination of $[\text{CpFe}(\text{CO})_2(\text{CH}_2\text{CH}_3)]$ are investigated by ab initio molecular orbital (MO), MP2 and density functional (DFT) calculations. © 1999 Elsevier Science S.A. All rights reserved.

Keywords: Molecular orbital; Density functional theory; Alkyls; β -Hydride elimination

1. Introduction

Transition metal alkyls are important because they are found or have been proposed as intermediates in many industrially significant homogenous and heterogeneous chemical processes. β -Hydride elimination and its reverse, alkene insertion, are particularly important reaction pathways for these species and have been the subject of many studies [1]. It has also been proposed that 1-alkene formation in the Fischer–Tropsch reaction occurs via a β -hydride elimination from an iron alkyl species [2].

The compounds of the type $[\text{Cp}^*\text{Fe}(\text{CO})_2\text{R}]$ ($\text{R} =$

CH_3 , CH_2CH_3 , ^iPr) have been previously reported along with some characterization data. This series of compounds represents easily accessible stable alkyl compounds ideal for reactivity and mechanistic studies of transition metal alkyl compounds. These compounds could be models for key intermediates in catalytic reactions. Previous work on the thermal decomposition of related iron alkyl compounds have shown, from the range of organic products, that the mechanism is non-trivial [3]. Recently reported work on palladium dialkyl compounds show that they too yield a range of products upon thermal decomposition [4]. A UV/Mass spectral study [5] has found two likely decomposition routes which are competitive for $[\text{CpFe}(\text{CO})_2(\text{CH}_2\text{CH}_3)]$ and $[\text{CpFe}(\text{CO})_2(\text{CH}_2\text{CH}_2\text{CH}_3)]$. The two routes are decomposition by cleavage of the iron–carbon bond resulting in two radicals, and β -hydride elimination. Although the alkene hydride complex was never detected, alkenes were seen in the product spectrum [5].

* Corresponding author. Fax: +27-21-6897499.

E-mail addresses: jrm@psipsy.uct.ac.za (J.R. Moss), knaidoo@psipsy.uct.ac.za (K.J. Naidoo)

¹ Also corresponding author.

In this study we extend a previous series of long-chain alkyl compounds [6] to their iron pentamethylcyclopentadienyl analogues and investigate the crystal and molecular structure of one such compound. Additionally we report preliminary results of calculations designed to give more information on the β -hydride elimination reaction of these compounds.

2. Experimental

2.1. General procedures

All reactions were carried out under nitrogen using standard Schlenk tube techniques. THF was distilled from sodium before use. The alkyl halides were obtained from the suppliers shown, with percentage purity in parentheses: *n*-C₃H₅Br (99), *n*-C₅H₁₁Cl (99), *n*-C₆H₁₃Cl (99), *n*-C₇H₁₅Cl (99), *n*-C₈H₁₇Br (99), *n*-C₉H₁₉Br (98), *n*-C₁₁H₂₃Br (99) from Aldrich; *n*-C₄H₉Br (99) from Riedel-de Haën; *n*-C₁₀H₂₁Br (98) from Merck and *n*-C₁₂H₂₅Br from Sigma. [Cp*Fe(CO)₂]₂ was obtained from Strem.

Alumina (BDH, active neutral, Brockman grade 1) was deactivated before use. Melting points were recorded on a Kofler hot-stage microscope (Reichert Thermovar) and are uncorrected. Microanalyses were performed by the University of Cape Town Microanalytical Laboratory. IR spectra were recorded on a Perkin–Elmer 983 spectrophotometer. ¹H- and ¹³C-NMR spectra were recorded either on a Varian XR 200 or a Varian Unity-400 spectrometer. Low-resolution mass spectra were recorded with a VG Micromass 16F spectrometer, operating at 70 eV ionizing voltage. The source temperature was raised from room temperature (r.t.) until the spectrum was observed.

Data for the X-ray diffraction studies were collected on an Enraf–Nonius CAD4 diffractometer at 233 K with graphite-monochromated Mo–K_α radiation.

2.2. Computational methods

Ab initio Hartree–Fock and MP2 molecular orbital (MO) calculations were carried out using the GAMESS [7a] program. Our approach to examining the potential energy surface (PES) of the reaction involved performing calculations with the MINI basis set [7b] for geometries. Linear interpolation of atomic coordinates coupled with geometry optimization was employed to estimate stationary points on the PES. Larger basis set ab initio calculations were performed with the SBK effective core potential basis set [7c,d] to determine the energies for key species.

Density functional (DFT) calculations were carried out using DMol [8]. All calculations were gradient corrected using the B88 (exchange) and LYP (correlation)

functionals with a frozen inner core. Geometry optimizations were calculated with no constraints using a double numeric basis set (DN). Numerical second derivative (Hessian) calculations were carried out to characterize stationary points. The energies of stationary points were calculated with a double numeric + polarization basis set (DNP). All calculations employed a fine numerical grid.

2.3. General method for the preparation of [Cp*Fe(CO)₂R] (Cp* = η⁵-C₅(CH₃)₅; R = *n*-C₃H₇ to *n*-C₁₂H₂₅)

A solution of Na[Cp*Fe(CO)₂] (5.6 mmol) in THF (20 ml) was added dropwise over 10 min to the alkyl halide (ca. 4.5 mmol) at 0°C with stirring. The solution was then stirred for a further 24 h at r.t. The solvent was removed under reduced pressure leaving a brown oily residue. This was extracted with hexane (3 × 40 ml), filtered and the solvent removed under reduced pressure yielding an orange oil with an almost quantitative crude yield. The oil was transferred to a deactivated alumina chromatography column and eluted with hexane. A yellow band was collected and the solvent removed under reduced pressure. The oil was then dried in vacuo. Yields and characterization data are given in Tables 2–5.

2.4. X-ray crystallography

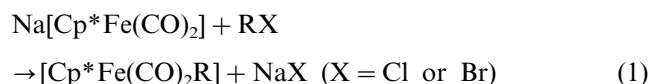
Yellow–orange crystals of [Cp*Fe(CO)₂(*n*-C₅H₁₁)] (**3**) were grown from a hexane solution kept in the dark at –10°C for 1 month. The crystals are monoclinic, *P*2₁/*c*, *a* = 8.304, *b* = 16.345, *c* = 12.568 Å, β = 91.43°, *V* = 1705.3218 Å³, *Z* = 4, *D*_{calc} = 1.24 Mg m^{–3}, *F*(000) = 679.96, λ(Mo–K_α) = 0.71069 Å, μ = 8.29 mm^{–1}, *T* = –35°C.

A crystal with dimensions 0.3 × 0.3 × 0.2 mm was used. Lattice parameters were determined by least-squares fitting of the setting angles of 25 reflections 1° ≤ θ ≤ 2.25° automatically centered on a CAD4 diffractometer. Intensities were collected with graphite-monochromated Mo–K_α radiation, ω–2θ scan mode, scan width (0.80 + 0.35 tan θ)°, aperture setting (1.12 + 1.05 tan θ) mm and 4 mm length, range of reflections 25° ≥ θ ≥ 1°. 3260 reflections were measured of which 2676 were unique, and 2108 of these were used in the refinement, index range *h* –9/9, *k* 0/19, *l* 0/14. Three intensity control reflections (–5 –2 7, 2 –12 2, –3 2 9) monitored every 120 reflections showed a 8.6% loss in intensity; no correction was applied. Data were corrected for background, scan speed, Lorentz and polarization effects. The iron atom was located using the Patterson function. The remainder of the structure was solved using SHELX-76 [11] and refined by difference Fourier methods using SHELX-86 [12]. The

final model included anisotropic refinement of all non-hydrogen atoms and isotropic refinement of hydrogens constrained to idealized positions with C–H = 1.00 Å which gave final $R = 0.095$, $wR = 0.095$, $w = 30.213/[\sigma^2(F_o)]$, $S = 36.57$, residual electron density $+0.33 \geq \Delta\rho \geq -0.38 \text{ e } \text{Å}^{-3}$.

3. Results and discussion

The alkyl compounds shown in Table 1 were all prepared by the same general route:



In the syntheses (Eq. (1)), an excess of $\text{Na}[\text{Cp}^*\text{Fe}(\text{CO})_2]$ was used to ensure that no alkyl halide remained at the end of the reaction because of difficulty in separating this from iron alkyl products. In this way the pure alkyl iron compounds could be

obtained in high yield (see Table 2). The compounds are yellow–brown oils or solids which are stable in air for a few hours for the oils, to a few days for the solids. Under a nitrogen atmosphere and in the dark, they can be kept for several months at -15°C without appreciable decomposition. This increased stability over the cyclopentadienyl analogues on exposure to heat, light and air, enables them to be used more easily in model studies of catalytic reactions, and in structural studies.

All new compounds were fully characterized by m.p., microanalyses, IR, ^1H -, ^{13}C -NMR and mass spectrometry (Tables 2–5).

3.1. IR spectra

All the compounds, **1–10**, show two strong $\nu(\text{CO})$ bands in their IR spectra in hexane solution at 1987 and 1933 cm^{-1} . For the analogous $[\text{Cp}\text{Fe}(\text{CO})_2\text{R}]$ compounds the $\nu(\text{CO})$ bands appear at 2008 and 1954 cm^{-1} [6], indicating that the C–O bond is weaker in the

Table 1

Compound	R
1	C_3H_7
2	C_4H_9
3	C_5H_{11}
4	C_6H_{13}
5	C_7H_{15}
6	C_8H_{17}
8	$\text{C}_{10}\text{H}_{21}$
9	$\text{C}_{11}\text{H}_{23}$
10	$\text{C}_{12}\text{H}_{25}$

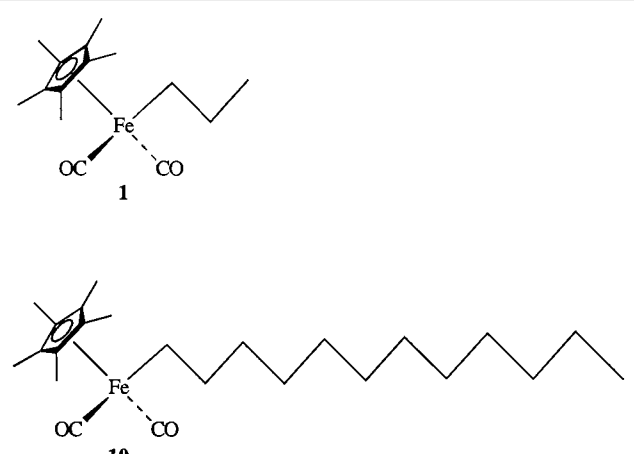


Table 2
Data for $\text{Cp}^*\text{Fe}(\text{CO})_2\text{R}$

Compound	R	Yield (%)	M.p. ($^\circ\text{C}$)	Elemental analysis ^a (%)	
				C	H
1	<i>n</i> - C_3H_7	83	76–82	62.38 (62.07)	7.68 (7.66)
2	<i>n</i> - C_4H_9	82	57–60	63.32 (63.16)	8.09 (7.95)
3	<i>n</i> - C_5H_{11}	93	31–32	64.49 (64.16)	8.34 (8.23)
4	<i>n</i> - C_6H_{13}	60	Oil	65.22 (65.07)	8.70 (8.50)
5	<i>n</i> - C_7H_{15}	81	Oil	65.90 (65.90)	8.05 (8.73)
6	<i>n</i> - C_8H_{17}	60	30–33	66.95 (66.65)	9.01 (8.97)
7	<i>n</i> - C_9H_{19}	88	Oil	67.55 (67.36)	9.40 (8.97)
8	<i>n</i> - $\text{C}_{10}\text{H}_{21}$	31	Oil	67.1 (68.02)	9.0 (9.36)
9	<i>n</i> - $\text{C}_{11}\text{H}_{23}$	90	Oil	68.25 (68.64)	9.20 (9.54)
10	<i>n</i> - $\text{C}_{12}\text{H}_{25}$	75	Oil	69.77 (69.21)	9.93 (9.70)

^a Calculated values in parentheses.

Table 3
¹H-NMR data for [Cp*Fe(CO)₂R]^a

R	C ₅ (CH ₃) ₅	Fe-CH ₂ ^c	(CH ₂) _x	CH ₃ ^b
CH ₃ ^{d,e}	1.45	–	–	0.08
C ₂ H ₅ ^e	1.72	1.03	–	1.25
<i>n</i> -C ₃ H ₇	1.71	0.95	1.48	0.92
<i>n</i> -C ₄ H ₉	1.71	0.94	1.36	0.87
<i>n</i> -C ₅ H ₁₁	1.72	0.94	1.26	0.86
<i>n</i> -C ₆ H ₁₃	1.71	0.94	1.27	0.87
<i>n</i> -C ₇ H ₁₅	1.71	0.94	1.26	0.86
<i>n</i> -C ₈ H ₁₇	1.71	0.93	1.25	0.86
<i>n</i> -C ₉ H ₁₉	1.71	0.94	1.25	0.86
<i>n</i> -C ₁₀ H ₂₁	1.72	0.95	1.26	0.88
<i>n</i> -C ₁₁ H ₂₃	1.70	0.94	1.24	0.86
<i>n</i> -C ₁₂ H ₂₅	1.71	0.94	1.24	0.86

^a Measured in CDCl₃ relative to TMS (δ 0.00 ppm).

^b The methyl protons are triplets (J = 6.6 Hz).

^c The α -methylene protons are triplets (J = 8.3 Hz).

^d Measured in C₆D₆ relative to TMS (δ 0.00 ppm).

^e Refs. [9,10].

[Cp*Fe(CO)₂R] compounds than in the [CpFe(CO)₂R] compounds; conversely, the Fe–CO bond is stronger in the [Cp*Fe(CO)₂R] compounds than in the [CpFe(CO)₂R] compounds. This effect is due to the increased electron density on the iron atom, from the Cp* ligand, which is donated into the π^* orbital of the CO, thus weakening the CO bond. There is no significant change in ν (CO) on changing the length of the alkyl chain in either the Cp or Cp* series.

3.2. NMR spectra

In the ¹H-NMR spectrum separate resonances were observed for the Cp* ring methyls and alkyl methyl protons; these showed no variation with alkyl chain length (see Table 3). The α -methylene protons appear separate from the other methylene protons, due to the electron density from the metal, and are further upfield than in the corresponding Cp compounds. The other methylene protons appear as a broad singlet, the integration being the only way to distinguish between compounds of differing alkyl chain length.

The ¹³C-NMR data for the compounds, **1–10**, are given in Table 4. Assignments were made by comparison with data reported for the short-chain compounds, and related long-chain compounds [CpFe(CO)₂R] [6,9,10]. The resonances for the Cp* carbons, Cp* methyl carbons, and the CO appear at the expected positions and are independent of the alkyl chain length. The resonance of the α -methylene carbon, which is a measure of relative electron density, varies from δ = –13.1 in the methyl complex to a maximum of δ = 17.00 in the *n*-propyl complex, and then decreases to δ = 14.11 ppm in the hexyl complex. The δ values for the α -methylene carbon on the higher homologues then

remain constant at $\delta \approx 14.12$ ppm. This effect is a magnified property of the alkyl chain (i.e. alkane) and has been shown to correlate with the alkyl migration rate in related compounds [13].

3.3. Mass spectra

All the compounds prepared showed parent molecular ions (M) in their mass spectra. The main fragmentation pathways are as follows: M, M – CO, M – 2CO, M – 2CO – H, M – 2CO – 2H, M – 2CO – 4H, M – 2CO – 6H.

3.4. Crystal and molecular structure of [Cp*Fe(CO)₂(*n*-C₅H₁₁)] (**3**)

[Cp*Fe(CO)₂(*n*-C₅H₁₁)] forms monoclinic crystals in the space group *P*2₁/*c*. Final atomic coordinates, anisotropic temperature factors, bond lengths and angles for **3** are given in Tables 6 and 7. The structure of the molecule and packing in the crystal are shown in Figs. 1 and 2.

The iron atom is pseudo-octahedrally coordinated to two carbonyls, the alkyl chain and the pentamethylcyclopentadienyl ligand. The alkyl chain lies in an extended staggered conformation (Fig. 1, view A) giving the molecule approximate C_v symmetry (Fig. 2, view B). The five carbons and iron are coplanar to within ± 0.02 Å, and the ten carbons of the pentamethylcyclopentadienyl ligand are coplanar to within ± 0.01 Å. The β -carbon of the alkyl chain lies in a conformation between the two CO ligands. This is in contrast to many other cyclopentadienyl iron dicarbonyl structures [14] where the β -carbon lies between a CO ligand and the cyclopentadienyl ring. Whether this conformational preference is caused by the pentamethylcyclopentadienyl ligand or by packing effects in the crystal is unclear. The iron to carbon bond in the alkyl chain was found to be 2.07 Å. This falls within the range (2.06–2.20 Å) of similar structures, which mainly contained a cyclopentadienyl ligand [14]. The iron carbon bond length (2.07 Å) thus shows remarkable insensitivity to the increased electron density going from the cyclopentadienyl compounds to the pentamethylcyclopentadienyl compound. This suggests that the greater instability of the analogous cyclopentadienyl compounds has more to do with the bonding of the ancillary ligands than with the strength of the Fe–C(alkyl) bond. Indeed recent photochemical studies of the iron acyl compounds $[(\eta^5\text{-C}_5\text{R}_5)\text{Fe}(\text{CO})(\text{PPh}_3)\text{COCH}_3]$ where R = H or CH₃ have shown that CO is lost exclusively for R = H, and PPh₃ is lost exclusively for R = CH₃ [15].

The molecules are arranged in layers with the alkyl chains of the molecule oriented in opposite directions in alternate layers. Within each layer the alkyl chains are

Table 4
 $^{13}\text{C-NMR}$ of $[\text{Cp}^*\text{Fe}(\text{CO})_2\text{R}]$ in CDCl_3 relative to TMS (δ 0.0 ppm)

R	Compound	CO	C_{Cp}	$\text{C}(\text{CH}_3)$	FeCH_2 (α)	C_2 (β)	C_3 (γ)	C_4 (δ)	C_5 (ϵ)	C_6	C_7	C_8	C_9	C_{10}	C_{11}	C_{12}
Methyl ^a	–	219.5	105.2	9.2	–13.1											
Ethyl ^a	–	219.5	94.8	9.3	6.72	21.6										
<i>n</i> -Propyl	1	–	94.79	9.34	17.00	30.28	20.16									
<i>n</i> -Butyl	2	–	94.66	9.23	13.60	40.02	28.58	13.86								
<i>n</i> -Pentyl	3	219.54	94.66	9.23	13.97	38.09	37.37	22.47	14.18							
<i>n</i> -Hexyl	4	219.61	94.74	9.31	14.11	37.79	35.61	31.83	22.84	14.16						
<i>n</i> -Heptyl	5	219.63	94.74	9.33	14.13	37.86	35.92	29.27	32.10	22.76	14.13					
<i>n</i> -Octyl	6	219.62	94.74	9.33	14.14	37.84	35.96	29.54	29.51	31.99	22.72	14.14				
<i>n</i> -Nonyl	7	219.61	94.74	9.32	14.12	37.84	35.94	29.80	29.56	29.41	31.96	22.71	14.12			
<i>n</i> -Decyl	8	219.61	94.72	9.31	14.12	37.84	35.95	29.84	29.73	29.57	29.36	31.93	22.69	14.12		
<i>n</i> -Undecyl	9	219.59	94.72	9.30	14.11	37.83	35.94	29.83	29.73	29.67	29.56	29.37	31.92	22.68	14.11	
<i>n</i> -Dodecyl	10	219.63	94.75	9.33	14.14	37.86	35.97	29.86	29.74	29.74	29.69	29.59	29.38	31.95	22.71	14.14

^a Refs. [9,10].

directed alternately upwards and downwards in the direction of the alkyl chain (see Fig. 2). There are no intermolecular interactions within the crystal.

3.5. Density functional calculations of the β -hydride elimination of $[\text{CpFe}(\text{CO})_2(\text{CH}_2\text{CH}_3)]$

$[\text{CpFe}(\text{CO})_2(\text{CH}_2\text{CH}_3)]$ was chosen to model the reaction as it is more convenient to perform calculations on, than the Cp^* analogues. The reaction scheme involves the loss of CO followed by β -hydride elimination (see Fig. 3). DFT investigation of the β -hydride elimination reaction of $[\text{CpFe}(\text{CO})_2(\text{CH}_2\text{CH}_3)]$ indicate that after the loss of one CO from the complex, the reaction proceeds without a barrier to form the ethylene hydride complex, $[\text{CpFe}(\text{CO})(\text{H})(\text{CH}_2\text{CH}_2)]$. Optimization of the monocarbonyl, $[\text{CpFe}(\text{CO})(\text{CH}_2\text{CH}_3)]$, from several starting conformations led to the product $[\text{CpFe}(\text{CO})(\text{H})(\text{CH}_2\text{CH}_2)]$. The transition state (TS) for the reaction therefore is likely to lie in the region of CO loss. Several attempts to find the TS were made. Starting structures for the optimizations were constructed in two ways. First the carbonyl-to-metal distance was varied from 1.76 to 2.8 Å to produce a series of starting TS structures. A second set of TS starting geometries was generated from intermediate structures generated from the interpolation of appropriate Z-matrix coordinates. Hessians were calculated numerically for each starting structure prior to optimization, periodically during optimization, and after optimization. In all cases the imaginary vibrational mode of the optimized structure turned out to be trivial (e.g. a rotation of the Cp ring). Each starting structure when optimized resulted in the ‘re-incorporation’ of the carbonyl ligand into the metal complex structure. The calculated energy difference between the reactant, $[\text{CpFe}(\text{CO})_2(\text{CH}_2\text{CH}_3)]$, and products of the reaction, $[\text{CpFe}(\text{CO})(\text{H})(\text{CH}_2\text{CH}_2)] + \text{CO}$, was calculated as +35.28 kcal mol⁻¹.

3.6. Molecular orbital calculations of the β -hydride elimination of $[\text{CpFe}(\text{CO})_2(\text{CH}_2\text{CH}_3)]$

We repeated the calculations using an ab initio approach (MP2). The results corresponded to our previous DFT predictions and the experimental results. However, the DFT structures correspond more closely with experimental structures than do those obtained by MP2. Once again we made several attempts to find the TS using starting structures which we described in the previous section. When we performed MP2 optimization calculations on the mono-carbonyl ethyl compound, $[\text{CpFe}(\text{CO})(\text{CH}_2\text{CH}_3)]$, to model the case of CO dissociation prior to β -hydride elimination, an agostic structure

Table 5
Mass spectral data for [Cp*Fe(CO)₂R]

Assignments	Relative peak intensities for compounds 1–10									
	1	2	3	4	5	6	7	8	9	10
Parent (M)	63	7	2	15	5	19	8	7	9	5
M–CO	–	17	17	20	18	–	30	19	18	8
M–2CO	–	2	–	3	–	–	24	–	–	–
M–2CO–H	–	22	17	20	21	–	–	24	37	27
M–2CO–2H	–	92	100	100	100	–	100	100	100	100
M–2CO–4H	–	8	7	17	22	–	–	–	–	25
M–2CO–6H	–	–	16	28	40	–	–	–	–	27
Cp*Fe(CO)H	–	5	4	6	7	–	13	–	9	8
Cp*FeH	–	7	4	5	6	–	–	–	5	4
Cp*Fe–H	–	100	96	50	66	–	32	48	50	39
Cp*–2H	100	26	22	23	27	100	25	25	8	17
C ₃ H ₇	–	–	9	5	45	54	–	25	14	18
CO	100	–	–	21	9	–	7	100	100	9

(i.e. an intermediate structure where the β -hydrogen is partially bonded to the iron and the β -carbon) was predicted. The structure was characterized as a minimum energy structure that was higher in energy than the optimized alkene hydride structure. We are investigating two metric parameters (C–H distance and M–M–C angle) as a function of the metal to (C–H bond) distance to further explore the MP2 produced agostic structure. The calculated energy difference between the reactant, [CpFe(CO)₂(CH₂CH₃)], and products of the reaction, [CpFe(CO)(H)(CH₂CH₂)] + CO, was calculated to be +38.80 kcal mol⁻¹, which is more than 3 kcal mol⁻¹ higher than the DFT calculation prediction.

3.7. Comparative performance of the molecular orbital and density functional calculations on structures along the β -hydride elimination reaction pathway

Ab initio MP2 and DFT calculations gave optimized structures of the reactant and product shown in Fig. 4. Calculated structures are compared with known crystal data in Tables 8 and 9. The DFT results were consistently closer to experimental findings than the results from Hartree–Fock (RHF) and RHF–MP2 calculations. All the DFT calculated bond lengths were within the range observed in X-ray crystal structures, except for the C=O bond of the carbonyl which was 0.01–0.02 Å longer than the experimentally observed bond lengths in both structures. The distance from the cyclopentadienyl carbons to the iron in [CpFe(CO)(H)(CH₂CH₂)] was calculated to be 0.02 Å longer than the experimental range observed for [(η^5 -C₅H₄CH₃)Fe(C₂H₄)₂] [16b], and the iron hydride bond was calculated to

be 0.02 Å shorter than that observed by neutron diffraction [17]. All bond angles were in good agreement with those observed in X-ray crystal structures. The structures obtained from Hartree–Fock calculations were not at all accurate as would be expected for applications of this level of theory to transition metal systems [18]. This is primarily due to the single determinant nature of the Hartree–Fock calculation.

Table 6
Fractional atomic coordinates ($\times 10^4$) and thermal parameters ($\text{Å}^2 \times 10^3$) with estimated S.D. values in parentheses for 3

Atom	x	y	z	U_{eq}^a
Fe(1)	1608(2)	2130(1)	1109(1)	35(1)
C(1)	4002(12)	2483(6)	1146(9)	42(4)
C(2)	4412(15)	3380(6)	1110(9)	51(4)
C(3)	6241(14)	3545(6)	1142(8)	45(4)
C(4)	6633(14)	4448(6)	1137(8)	45(4)
C(5)	8455(15)	4605(7)	1130(10)	58(4)
C(6)	–104(12)	1289(6)	1650(8)	37(3)
C(7)	1474(13)	1082(6)	2073(8)	40(4)
C(8)	2443(15)	904(6)	1210(8)	47(4)
C(9)	1477(17)	1028(6)	266(8)	53(5)
C(10)	–59(17)	1254(6)	524(9)	53(4)
C(11)	–1555(14)	1474(8)	2290(10)	58(5)
C(12)	1922(20)	996(8)	3225(8)	68(5)
C(13)	4137(15)	570(7)	1294(10)	62(5)
C(14)	2121(20)	883(8)	–862(9)	69(5)
C(15)	–1471(16)	1388(8)	–230(11)	65(5)
C(16)	1247(14)	2782(6)	36(9)	48(4)
C(17)	1199(12)	2824(7)	2129(8)	39(3)
O(1)	927(11)	3179(5)	–697(6)	64(3)
O(2)	960(12)	3280(5)	2791(7)	71(4)

^a Equivalent isotropic U calculated from anisotropic U : $U_{\text{eq}} = \frac{1}{3} \sum_i \sum_j U_{ij} a_i^* a_j^*$.

Table 7
Bond lengths (Å) and angles (°) for 3

Fe(1)–C(1)	2.069(10)	C(6)–C(7)	1.442(15)
Fe(1)–C(6)	2.102(10)	C(6)–C(10)	1.418(15)
Fe(1)–C(7)	2.103(10)	C(6)–C(11)	1.496(16)
Fe(1)–C(8)	2.123(10)	C(7)–C(8)	1.397(15)
Fe(1)–C(9)	2.091(10)	C(7)–C(12)	1.492(15)
Fe(1)–C(10)	2.110(12)	C(8)–C(9)	1.430(16)
Fe(1)–C(16)	1.739(11)	C(8)–C(13)	1.510(17)
Fe(1)–C(17)	1.751(11)	C(9)–C(10)	1.375(19)
C(1)–C(2)	1.508(14)	C(9)–C(14)	1.546(16)
C(2)–C(3)	1.542(17)	C(10)–C(15)	1.505(19)
C(3)–C(4)	1.512(14)	C(16)–O(1)	1.153(13)
C(4)–C(5)	1.535(17)	C(17)–O(2)	1.139(14)
C(16)–Fe(1)–C(17)	97.93(51)	Fe(1)–C(6)–C(11)	127.03(77)
C(10)–Fe(1)–C(17)	123.82(49)	Fe(1)–C(6)–C(10)	70.64(62)
C(10)–Fe(1)–C(16)	92.65(49)	Fe(1)–C(6)–C(7)	69.98(58)
C(9)–Fe(1)–C(17)	156.95(47)	C(10)–C(6)–C(11)	125.90(101)
C(9)–Fe(1)–C(16)	97.42(47)	C(7)–C(6)–C(11)	125.86(94)
C(9)–Fe(1)–C(10)	38.20(48)	C(7)–C(6)–C(10)	108.18(93)
C(8)–Fe(1)–C(17)	129.53(44)	Fe(1)–C(7)–C(6)	69.90(57)
C(8)–Fe(1)–C(16)	132.41(46)	C(6)–C(7)–C(12)	125.57(98)
C(8)–Fe(1)–C(10)	65.89(42)	C(6)–C(7)–C(8)	107.37(90)
C(8)–Fe(1)–C(9)	39.66(39)	Fe(1)–C(7)–C(12)	128.27(76)
C(7)–Fe(1)–C(17)	95.27(43)	Fe(1)–C(7)–C(8)	71.49(58)
C(7)–Fe(1)–C(16)	159.31(47)	C(8)–C(7)–C(12)	126.82(107)
C(7)–Fe(1)–C(10)	66.73(40)	Fe(1)–C(8)–C(7)	69.90(58)
C(7)–Fe(1)–C(9)	65.63(39)	C(7)–C(8)–C(13)	125.07(95)
C(7)–Fe(1)–C(8)	38.61(39)	C(7)–C(8)–C(9)	107.01(102)
C(6)–Fe(1)–C(17)	92.36(44)	Fe(1)–C(8)–C(13)	130.36(75)
C(6)–Fe(1)–C(16)	123.12(49)	Fe(1)–C(8)–C(9)	68.96(57)
C(6)–Fe(1)–C(10)	39.34(42)	C(9)–C(8)–C(13)	127.70(97)
C(6)–Fe(1)–C(9)	64.79(40)	Fe(1)–C(9)–C(8)	71.38(57)
C(6)–Fe(1)–C(8)	65.58(39)	C(8)–C(9)–C(14)	122.64(115)
C(6)–Fe(1)–C(7)	40.13(39)	C(8)–C(9)–C(10)	110.31(95)
C(1)–Fe(1)–C(17)	90.38(47)	Fe(1)–C(9)–C(14)	125.58(76)
C(1)–Fe(1)–C(16)	89.63(48)	Fe(1)–C(9)–C(10)	71.63(62)
C(1)–Fe(1)–C(10)	144.92(43)	C(10)–C(9)–C(14)	127.00(113)
C(1)–Fe(1)–C(9)	106.82(45)	C(6)–C(10)–C(9)	107.10(99)
C(1)–Fe(1)–C(8)	106.82(45)	Fe(1)–C(10)–C(9)	70.16(68)
C(1)–Fe(1)–C(7)	87.12(43)	Fe(1)–C(10)–C(6)	70.01(61)
C(1)–Fe(1)–C(6)	106.19(42)	C(9)–C(10)–C(15)	127.11(109)
Fe(1)–C(1)–C(2)	119.23(72)	C(6)–C(10)–C(15)	125.68(107)
C(1)–C(2)–C(3)	113.05(83)	Fe(1)–C(10)–C(15)	128.00(77)
C(2)–C(3)–C(4)	112.44(91)	Fe(1)–C(16)–O(1)	175.41(99)
C(3)–C(4)–C(5)	112.07(88)	Fe(1)–C(17)–O(2)	178.81(99)
–	–	–	–

Consequently we extended our calculations to the MP2 level where the structures obtained from MP2 calculations were generally in agreement with similar structures determined by X-ray crystallography (see Tables 8 and 9). However, the DFT-obtained structures compared better with experimental values than did the MP2-derived structures. In particular the position of the hydride in the MP2-determined structure of $[\text{CpFe}(\text{CO})(\text{H})(\text{CH}_2\text{CH}_2)]$ may be too close to the cyclopentadienyl ring. This has the effect of distorting the usual tripod ligand arrangement typically observed in structures of the type $[\text{CpFe}(\text{L})(\text{L}')(\text{L}'')]$ (see Fig. 4).

The structural differences observed for the MP2 calculations may in part be due to the small basis set that had to be used to make the calculations feasible on a desktop workstation capable of 775 MIPS.

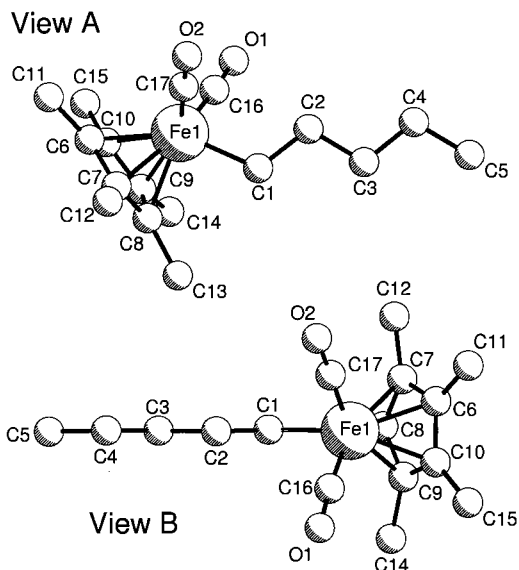


Fig. 1. Molecular structure of $[\text{Cp}^*\text{Fe}(\text{CO})_2(n\text{-C}_5\text{H}_{11})]$ showing the staggered alkyl chain (view A), and the mirror plane in the molecule (view B).

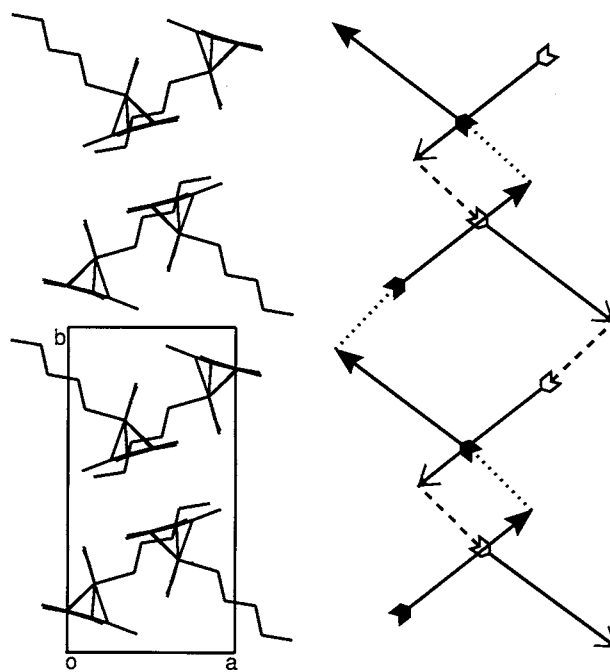
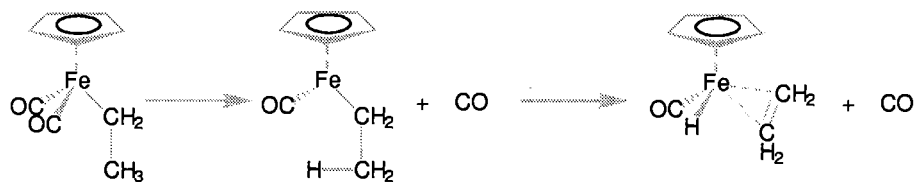
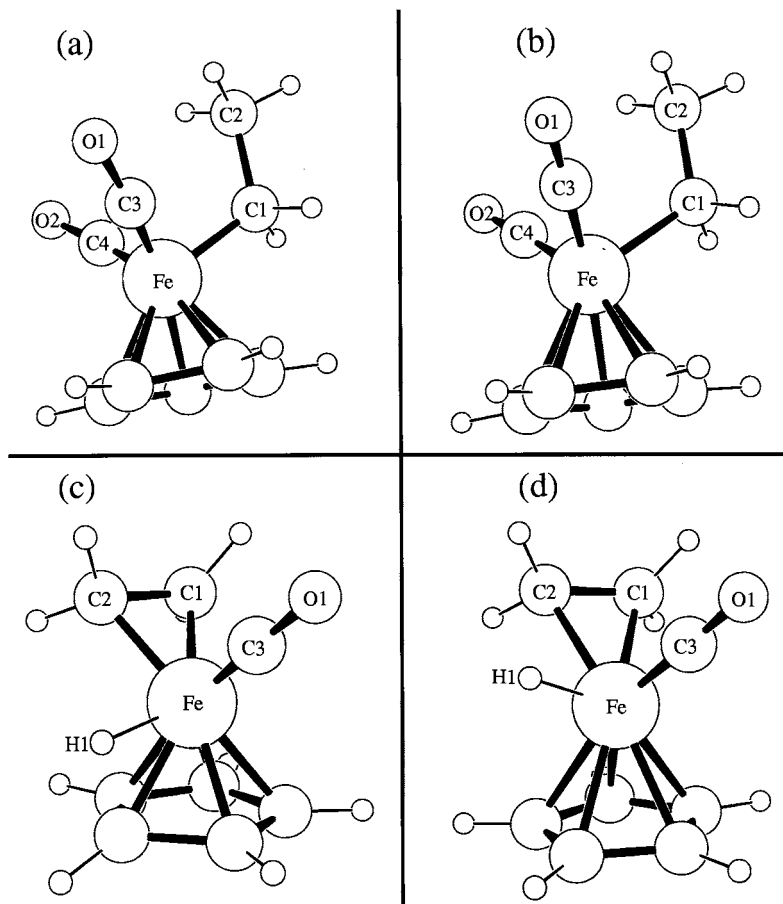


Fig. 2. Crystal structure of $[\text{Cp}^*\text{Fe}(\text{CO})_2(n\text{-C}_5\text{H}_{11})]$ viewed down the *c*-axis, showing the alternating arrangement of the alkyl chain (with accompanying schematic).

Fig. 3. Loss of CO followed by β -hydride elimination.Fig. 4. Optimized structures of $[\text{CpFe}(\text{CO})_2(\text{CH}_2\text{CH}_3)]$ calculated by: (a) MO-RHF-MP2 and (b) DFT; and optimized structures of $[\text{CpFe}(\text{CO})(\text{H})(\text{CH}_2\text{CH}_2)]$ calculated by: (c) MO-RHF-MP2 and (d) DFT.

The MP2 calculations predicted structures where the iron to carbon bonds were shorter than those obtained by DFT calculations. Both the iron to alkyl carbon bond and the iron to carbonyl bond lengths were shorter than the experimental values, while the carbon to oxygen bonds of the carbonyl were seen to be greater than the experimentally observed values (Table 8). Furthermore, this relative difference between experimentally observed and ab initio (MP2) predicted iron-carbon and carbon-oxygen bonds, was also seen in the alkene hydride structure (see Table 9).

DFT calculations produced structures for both the ethyl compound and the alkene hydride compounds, which were in very good agreement with the X-ray

crystal structural data obtained on related compounds. Furthermore, for the study of this reaction, the method appears to be superior to the RHF-MP2 method for similar computational effort. We found that correlation effects are significant in the system studied, especially in the case of the alkene hydride, $[\text{CpFe}(\text{CO})(\text{H})(\text{CH}_2\text{CH}_2)]$, where their inclusion is essential to obtain a reasonable structure. The DFT calculation, which predicts the reaction to be endothermic along a path that proceeds with no barrier to rearrangement to form the alkene hydride complex, once the CO has been removed appears to be in line with UV/mass spectral studies performed on these compounds [5].

Table 8

Comparison of calculated bond lengths (Å) and angles (°) for [CpFe(CO)₂(CH₂CH₃)] with experimental data

Bond/angle	MO–RHF–MP2	DFT	Exp. ^a	Exp. Ref.
Fe–C ₁	1.94	2.13	2.06–2.20	[14]
Fe–C ₃	1.58	1.76	1.72–1.79	[14]
Fe–C ₄	1.58	1.76	1.67–1.86	[14]
C ₃ –O ₁	1.28	1.20	1.14–1.19	[14]
C ₄ –O ₂	1.28	1.20	1.15–1.19	[14]
C ₁ –C ₂	1.59	1.55	1.51–1.55	[14]
Fe–C _{Cp}	2.05–2.08	2.22–2.23	2.07–2.26	[14]
C ₃ –Fe–C ₄	91.4	96.5	89.2–95.0	[14]
C ₁ –Fe–C ₃	92.0	89.4	88.0–94.2	[14]
Fe–C ₃ –O ₁	174.4	177.0	177.5–178.8	[14]
Fe–C ₁ –C ₂	117.4	118.8	113.3–119.2	[14]

^a Values from X-ray structural data.

Table 9

Comparison of calculated bond lengths (Å) and angles (°) for [CpFe(CO)(H)(CH₂CH₂)] with experimental data

Bond/angle	MO–RHF–MP2	DFT	Exp. ^a	Exp. Ref.
Fe–C ₁	1.93	2.13	2.02–2.32	[16a–g]
Fe–C ₂	1.95	2.14	2.02–2.32	[16a–g]
Fe–C ₃	1.58	1.74	1.74–2.00	[16b,c,f,g]
C ₃ –O ₁	1.28	1.20	1.11–1.18	[16b,c,f,g]
Fe–C _{Cp}	1.99–2.14	2.14–2.17	2.06–2.12	[16b]
C ₁ –C ₂	1.50	1.43	1.36–1.43	[16a–g]
Fe–H ₁	1.55	1.52	1.54–1.62 ^b	[17]

^a Values from X-ray structural data.

^b Neutron diffraction data.

Our inability to locate the TS by both DFT and ab initio MP2 level of theory may be either due to an inappropriate theoretical model (i.e. small basis set) or environmental effects. To increase the basis set of the MP2 calculations substantially would put the calculations out of reach of standard desktop workstations, which are now primarily used for these calculations. Since the electrostatic field provided by the solvent, THF, might play a minor but energetically significant role in the reaction, we believe that locating the TS would be possible if we included this effect. We are presently investigating a mean field approach to simulate solvent inclusion.

Acknowledgements

We thank UCT and the FRD for support; Leonard Barbour for X-ray crystal data collection, and Mino

Caira for invaluable advice during the X-ray structural studies.

References

- [1] (a) G.M. Whitesides, J.F. Gaasch, E.R. Stedronsky, *J. Am. Chem. Soc.* 94 (1972) 5258. (b) J.W. Lauher, R. Hoffmann, *J. Am. Chem. Soc.* 98 (1976) 1729. (c) F. Delbecq, *Organometallics* 9 (1990) 2223. (d) A. Fiedler, D. Schröder, W. Zummack, H. Schwarz, *Inorg. Chim. Acta* 259 (1997) 227.
- [2] W.A. Herrmann, *Angew. Chem. Int. Ed. Engl.* 21 (1982) 117.
- [3] D.L. Reger, E.C. Culbertson, *Inorg. Chem.* 16 (1977) 3104.
- [4] J.W. Keister, E.J. Parsons, *J. Organomet. Chem.* 487 (1995) 23.
- [5] J.A. Bartz, T.M. Barnhart, D.B. Galloway, L.G. Heuy, T. Glenewinkel-Meyer, R.J. McMahon, F.F. Crim, *J. Am. Chem. Soc.* 115 (1993) 8389.
- [6] A. Emeran, M.A. Gafoor, J.K.I. Goslett, Y.-H. Liao, L. Pimble, J.R. Moss, *J. Organomet. Chem.* 405 (1991) 237.
- [7] (a) M.W. Schmidt, K.K. Baldrige, J.A. Boatz, S.T. Elbert, M.S. Gordon, J.H. Jensen, S. Koseki, N. Matsunaga, K.A. Nguyen, S.J. Su, T.L. Windus, M. Dupuis, J.A. Montgomery, *J. Comp. Chem.* 14 (1993) 1347. (b) S. Huzinaga, J. Andzelm, M. Klobukowski, E. Radzio-Andzelm, Y. Sakai, H. Tatewaki, *Gaussian Basis Sets for Molecular Calculations*, Elsevier, New York, 1984. (c) H. Basch, M. Krauss, W.J. Stevens, *J. Phys. Chem.* 81 (1984) 6026. (d) H. Basch, P.G. Jasien, M. Krauss, W.J. Stevens, *Can. J. Chem.* 70 (1992) 612.
- [8] DMol, Version 2.36, Density Functional Theory Electronic Structure Program, Biosym. Technologies, Inc., 1994.
- [9] D. Catheline, D. Astruc, *J. Organomet. Chem.* 226 (1982) C52.
- [10] C. Roger, M.-J. Tudoret, V. Guerchais, C. Lapinte, *J. Organomet. Chem.* 365 (1989) 347.
- [11] G.M. Sheldrick, The SHELX program, in: H. Schenk, R. Oltof-Hazenkamp, J. van Koningsveld, G.C. Bassi (Eds.), *Computing in Crystallography*, Delft University Press, The Netherlands, 1978, p. 34.
- [12] G.M. Sheldrick, in: G.M. Sheldrick, C. Krüger, R. Goddard (Eds.), *Computing in Crystallography*, vol. 3, Oxford University Press, London, 1985, p. 175.
- [13] (a) J.-A. Andersen, Ph.D. Thesis, University of Cape Town, 1994. (b) J.R. Moss, J.-A.M. Andersen, R. George, *J. Organomet. Chem.* 505 (1995) 131.
- [14] (a) L. Pope, P. Sommerville, M. Laing, K.J. Hindson, J.R. Moss, *J. Organomet. Chem.* 112 (1976) 309. (b) V.B. Ribakov, L.A. Aslanov, V.M. Ionov, S.A. Eremin, *Zh. Strukt. Khim.* 24 (1983) 100. (c) J.K.P. Ariyaratne, A.M. Bierrum, M.L.H. Green, C.K. Prout, M.G. Swanwick, *J. Chem. Soc. A* (1969) 1309. (d) T.C.T. Chang, T.S. Coolbaugh, B.M. Foxman, M. Rosenblum, N. Simms, C. Stockman, *Organometallics* 6 (1987) 2394. (e) [Cp*Fe(CO)₂(*n*-C₅H₁₁)] in this paper.
- [15] S.G. Davies, W.C. Watkins, *J. Chem. Soc. Chem. Commun.* (1994) 491.
- [16] (a) T.C.T. Chang, B.M. Foxman, M. Rosenblum, C. Stockman, *J. Am. Chem. Soc.* 103 (1981) 7361. (b) U. Zenneck, W. Frank, *Angew. Chem. Int. Ed. Engl.* 25 (1986) 831. (c) H. Hoberg, K. Jenni, K. Angermund, C. Kruger, *Angew. Chem. Int. Ed. Engl.* 26 (1987) 153. (d) A.R. Luxmoore, M.R. Truter, *Acta Crystallogr.* 15 (1962) 1117. (e) E. Linder, E. Schauss, W. Hiller, R. Fawzi, *Chem. Ber.* 118 (1985) 3915. (f) M. Brookhart, W.A. Chandler, A.C. Pfister, C.C. Santini, P.S.

- White, *Organometallics* 11 (1992) 1263. (g) F. Meier-Brocks, R. Albrecht, E. Weiss, *J. Organomet. Chem.* 439 (1992) 65.
- [17] (a) R. Bau, M.Y. Chiang, D.M. Ho, S.G. Gibbins, T.J. Emge, T.F. Koetzle, *Inorg. Chem.* 23 (1984) 2823. (b) J.S. Ricci, T.F. Koetzle, M.T. Bautista, T.M. Hofstede, R.H. Morris, J.F. Sawyer, *J. Am. Chem. Soc.* 111 (1989) 8823.
- [18] (a) J. Almhöf, J.H. Ammeter, K. Faegri, H.P. Lüthi, *J. Chem. Phys.* 77 (1982) 2002. (b) J. Almhöf, C. Park, *J. Chem. Phys.* 95 (1991) 1829.